Journal of Mathematical Modeling and Fractional Calculus

Website: https://acspublisher.com/journals/index.php/jmmfc

Received:10-11-2025, **Revised:** 20-12-2025
Accepted:29-12-2025, **Publication:** 30-12-2025
https://doi.org/10.48165/jmmfc.2025.2207, 2(2),117-133

Nanofluid flow, heat and mass transfer over a linear stretching surface under convective boundary conditions by considering MHD and chemical reaction effects is three-dimensional

Shakeel Ahmad[1], Attia Rani[2], Anosha Iram[1], Muhammad Sohail[1]

[1]Institute of Mathematics, Khwaja Fareed University of Engineering & Information Technology, Rahim Yar Khan 64200, Pakistan.
[2]Department of Mathematics, University of Wah, Wah Cantt., 47040, Pakistan.
Corresponding author Email: muhammad_sohail111@yahoo.com

Abstract:

This paper addresses Transport of heat and flow in 3 −dimensions behaviour of a Williamson nanofluid flowing across a porous layer for extending under the influence of magneto hydrodynamic (MHD) forces, heat rays, Darcy Forchheimer resistance, and chemical reaction influence. The governing nonlinear partial differential equations were abridged to similarity transformations into ordinary differential equations and to solve them systematically by the optimum Technique of homotopy investigation (OHAM). Effects of thermophoresis, Brownian motion, Deborah number, Prandtl number, porosity factor, Forchheimer number, and chemical reaction in addition radiation parameters taking place velocity, temperature and concentration profiles were studied in detail. It shows that velocity field is reducing in porosity, Forchimmer number, and magnetic parameter whereas stretching parameter improves the flow. Moreover, porous and inertial effects suppress the drag forces but the Williamson parameter enhances them. Larger values of Prandtl number, Chemical reactions with rays increase the rate of heat transfer whereby, the Brownian principle and thermophoretic diffusion reduces it.

Keywords: Chemical reactions; magneto hydrodynamic (MHD); Williamson fluid; OHAM.

1. Intorduction

The non-Newtonian fluids are extensively applied in fluid dynamics. For example, some common are petroleum, biological sciences, chemical industries and geophysics applications in a variety of trades. Owing to such applications, researches within the variety of non-Newtonian, the attention has been given to fluids. These flows are observed in plastics and food production,

Polymer working, ice and magma flow, biological fluids, Spinning of copper, extrusion and cord drawing. Important effects to fluid flow on an extending surface. Rasool et al. [1] involved numerical analysis of the MHD viscoelastic minuscule liquid on non-linear stretchy sheets embedded on a pore medium. Rasool et al. [2] investigated nonliquid flow in the MHD DarcyForchheimer fluid by means of a nonlinear, surface Darcy-Forchheimer of a Maxwell nanofluid, dual stratification. Locomotion across an extended surface was explored. Anwar et al. [3] beneath the effects of an orientated magnetic ground. In this work, the movement structure is adjusted to contain both Thermal expansion and condensation by taking the respective elements in the energy equation. Akbar and Sohail [4] studied the magneto hydrodynamic real fluid flow at $3D$ that integrates heat. Radiation and impacts of viscous dissipation, the consequences of buoyancy and viscous dispersal on $3D$ magnetohydrodynamic sticky combined small liquids ($MgO\ TiO_2$) under slip circumstances were studied. Rasool et al. Rasool et al. [5] studied a motion of Nano fluidics over nonlinearly convective spreadsheet in addition radiative Riga plate boundary conditions, correspondingly. The concept of mass various articles is written about transport. Khan et al. [6] applied the homotopy analysis technique to analyses the transmission of warmth of the Maxwell nanofluid above a uniformly pattern cylinder with convective warmth transport. As they claim, the curvature parameter exerts the similar effect on the rate of nanoliquid, warmth as well as focus. But the action of heat origin, fluid loss, and warmth, Joule heating substance. Things of the reaction were not considered. Khan et al. [7] shown theoretical examination of the bioconvection flow of Williamson nanoparticles over a vibrating tectonic plate. Saeed et al. Saeed et al. [8] investigated on the composite nanoparticles movement across is known as Darcy-Forchheimer flow permeable lengthened cylinder. Ali et al. [9] examined a number of adverse effects of MHD Maxwell nanofluid movement by obeying a passable stretching sheet, thermo-diffusion and radiation, no chemical reactions, finite part modeling. Ali et al. It was found that the MHD transportation is unstable. Ali et al. [10] study of spinning Maxwell spin of nanofluid on a stretchable slip with Cattaneo-Christov duple dispersal and energy of activation. Ali et al. [11-12] analysed the speed of an exponentially infinite vertical permeable time-independent Caisson fluid sheet. How various factors affect velocity, temperature, concentration, Nuseelt number and friction of the skin are talked about. Such random wave of these nanoparticles within the flowing fluid is referred to as Brownian motion. It is known that the agent determining thermal performance of nanoparticles in nanofluids is Brownian motion. Wakif et al. [13] as a more realistic means of optimizing the improvement in transferring heat by passively controlling the Nanofluids with nanomaterials. Abdelsalam and

Sohail [14] examined the bidirectional bio-convective stretched flow with combined thermo physical properties. They obtained the resulting smaller PDEs when using the theory of boundary layers. OHAM tool was used to add appropriate transformation to the converted ODEs of PDEs. They determined that the higher order approximations decrease the error. They documented the loss in velocity field versus magnetic parameter and magnetic upsurge in temperature profile. Moreover, we find decrease in concentration profile with Schmidt number. Mixing of grapheme Unsteady model of nanoparticles in Eyring Powell MHD momentum slip past over an extended sheet was examined. Uddin et al. [15] but very not many authors made an attempt to resolve the fluid flow of nanoparticles hybrid flow delinquent through novel numerical techniques. The issue in this article is $3-D$ flow of MHD hybrid Nano fluid over a sheet in existence which is extendable is investigated by the authors of thermal radiation. Hayat et al. [16] the mechanism via which radiation is released is called thermal radiation in every direction of a surface. There are many applications of thermal radiations in engineering and heat transfer analysis. In the conduction and convection, energy transfer among substances varies almost solely by the temperature. In the case of natural free convection, or when variable there are property effects, the strength of the temperature difference can stay a little greater than one, and can reach two. Shah et al. [17] have investigated rotating system of MHD nanofluid. Arguably, in the revelation of the above literature survey and applications we were going to learn a rotating $3-$dimensional movement of electro- MHD CNTS nanofluid across an encompassing porous sheet with thermal radiation. Wakif et al. [18] to reveal the shape of nanoparticles has an effect on slipping MHD convective flow of water-alumina nano liquid in a disc of zero mass flux that is rotating horizontally. At the same nanofluid method.

Our detailed review of the literature indicates a lack of previous investigations on the examination of three-dimensional Williamson fluid flow along a porous sheet for extending under the influence of magneto hydrodynamic (MHD). The modified non-linear and associated calculations have been solved using the OHAM.

2. Problem Formulation

Assume that a linear stretching sheet is passed by the unsteady three-dimensional incompressible Williamson fluid. Following is the continuity, momentum, temperature and concentration equation. The horizontal direction is represented by the x-axis the upward direction by the z-axis and the y-axis is perpendicular to both axes. The surface is stretching

along the *x*-axis with velocity $\mathcal{p} = U_{\mathfrak{r}} = ax$ and along the *y*-axis with velocity $\mathcal{q} = V_{\mathfrak{r}} = \mathcal{b}y$ as shown Fig. 1. Inclined magnetic field B_0 to the axis of rotation is working.

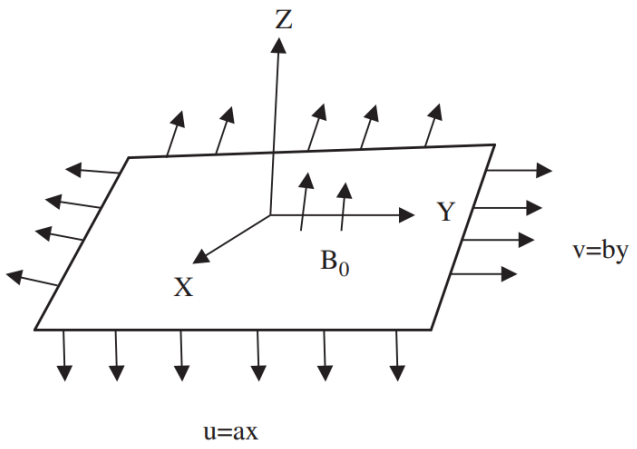

Fig. 1. Physical configuration and coordinate system of considered problem

$$\frac{\partial \mathcal{p}}{\partial x} + \frac{\partial \mathcal{q}}{\partial y} + \frac{\partial \mathfrak{r}}{\partial z} = 0, \tag{1}$$

$$\mathcal{p}\frac{\partial \mathcal{p}}{\partial x} + \mathcal{q}\frac{\partial \mathcal{p}}{\partial y} + \mathfrak{r}\frac{\partial \mathcal{p}}{\partial z} = \mathcal{q}\frac{\partial^2 \mathcal{p}}{\partial z^2} + \sqrt{2}\mathcal{p}\mathrm{r}\frac{\partial \mathcal{p}}{\partial z}\frac{\partial^2 \mathcal{p}}{\partial z^2} - \frac{\sigma {\beta_o}^2}{\rho}\mathcal{p} - \frac{\nu^*}{k^*}\mathcal{p}, \tag{2}$$

$$\mathcal{p}\frac{\partial \mathcal{q}}{\partial u} + v\frac{\partial \mathcal{q}}{\partial y} + \mathfrak{r}\frac{\partial \mathcal{q}}{\partial z} = \mathcal{q}\frac{\partial^2 \mathcal{q}}{\partial z^2} + \sqrt{2}\mathcal{q}\mathrm{r}\frac{\partial \mathcal{q}}{\partial z}\frac{\partial^2 \mathcal{q}}{\partial z^2} - \frac{\sigma {\beta_o}^2}{\rho}\mathcal{q} - \frac{\nu^*}{k^*}\mathcal{q}, \tag{3}$$

$$\mathcal{p}\frac{\partial \dot{\mathrm{T}}}{\partial x} + \mathcal{q}\frac{\partial \dot{\mathrm{T}}}{\partial y} + \mathfrak{r}\frac{\partial \dot{\mathrm{T}}}{\partial z} \tag{4}$$

$$= \frac{K}{\rho \hat{\mathrm{C}}_p}\frac{\partial^2 \dot{\mathrm{T}}}{\partial z^2} - \frac{\partial q\mathcal{r}}{\partial z} + \tau_1\left[D_B\frac{\partial \hat{\mathrm{C}}}{\partial z}\frac{\partial \dot{\mathrm{T}}}{\partial z} + \frac{D_{\dot{\mathrm{T}}}}{\dot{\mathrm{T}}_\infty}\left(\frac{\partial \dot{\mathrm{T}}}{\partial z}\right)^2\right] - Cr(C - C\infty),$$

$$\mathcal{p}\frac{\partial \hat{\mathrm{C}}}{\partial x} + \mathcal{q}\frac{\partial \hat{\mathrm{C}}}{\partial y} + \mathfrak{r}\frac{\partial \hat{\mathrm{C}}}{\partial z} = D_B\left(\frac{\partial^2 \hat{\mathrm{C}}}{\partial z^2}\right) + \frac{D_{\dot{\mathrm{T}}}}{\dot{\mathrm{T}}_\infty}\left(\frac{\partial^2 \dot{\mathrm{T}}}{\partial z^2}\right). \tag{5}$$

In Equations $(1)-(3), \mathcal{p}$ shows the velocity element voguish the $x-$guidance $\mathcal{q}$ is in the $y-$ guidance and $\mathfrak{r}$ is in the $z-$ guidance, G symbolizes Williamson fluid and n shows the flow rate of kinematic motion. In Equations $(4)\ and\ (5), k$ represents the heat permeability, T is the heat, r is how thick it is in motion, $\hat{\mathrm{C}}_p$ is the amount of space for radiation, τ_1 symbolizes the thermal capability rate, D_B is a measure of Brownian motion, $D_{\dot{\mathrm{T}}}$ the temperature gradient parameter is shown and $\mathcal{q}\mathrm{r}$ is the flow of radiation heat, which is defined as [19].

$$q\mathcal{r} = -\frac{4\sigma^*}{3K^*}\frac{\partial \dot{\mathrm{T}}^4}{\partial z}. \tag{6}$$

Where σ^*, k is the coefficient of absorption, and Stefan Boltzmann constant respectively. As $\dot{\mathrm{T}}^4 = 4\dot{\mathrm{T}}_\infty^3\dot{\mathrm{T}} - 3\dot{\mathrm{T}}_\infty^4$, Putting this into equation (4), it reduces to

$$\wp\frac{\partial\dot{\mathrm{T}}}{\partial x} + q\frac{\partial\dot{\mathrm{T}}}{\partial y} + \aleph\frac{\partial\dot{\mathrm{T}}}{\partial z} = \frac{K}{\rho\hat{\mathrm{C}}_p}\left(1 + \frac{4\sigma^*\dot{\mathrm{T}}_\infty^3}{K^*}\right)\frac{\partial^2\dot{\mathrm{T}}}{\partial z^2} + \tau_1\left[D_B\frac{\partial\hat{\mathrm{C}}}{\partial z}\frac{\partial\dot{\mathrm{T}}}{\partial z} + \frac{D_{\dot{\mathrm{T}}}}{\dot{\mathrm{T}}_\infty}\left(\frac{\partial\dot{\mathrm{T}}}{\partial z}\right)^2\right]. \tag{7}$$

Here are the equivalent boundary requirements for the aforementioned issue:

$$\wp = U_\aleph = ax, \qquad q = V_\aleph = \beth y, -k\frac{\partial\dot{\mathrm{T}}}{\partial z} = \hbar_f\left(\dot{\mathrm{T}}_f - \dot{\mathrm{T}}\right), -D_B\frac{\partial\hat{\mathrm{C}}}{\partial z} = \hbar_s\left(\hat{\mathrm{C}}_s - \hat{\mathrm{C}}\right) at\ \xi = 0, \wp \to 0, \qquad q \to 0, \aleph \to 0, \dot{\mathrm{T}} \to \dot{\mathrm{T}}_\infty, \hat{\mathrm{C}} \to \hat{\mathrm{C}}_\infty, \xi \to \infty. \tag{8}$$

$U_\aleph$ and $V_\aleph$ are significant values, while a and b are the bending rates. $c = \frac{a}{b}$, $\hbar_f, \hbar_s$ The factors of mass transport and radiative heat, $\dot{\mathrm{T}}_f$ the rising liquid warmth and $\hat{\mathrm{C}}$ is the attentiveness beneath the touching page in the above equation.

Based on equations above, likeness components are given as.

$$\wp = axf'(\xi), q = \beth yg'(\xi), \aleph = -(aq)^{1/2}\left(f(\xi) + \hat{\mathrm{C}}g(\xi)\right), \theta(\xi) = \frac{\dot{\mathrm{T}} - \dot{\mathrm{T}}_\infty}{\dot{\mathrm{T}}_f - \dot{\mathrm{T}}_\infty}, \varphi(\xi) = \frac{\hat{\mathrm{C}} - \hat{\mathrm{C}}_\infty}{\hat{\mathrm{C}}_f - \hat{\mathrm{C}}_\infty}, \xi = \daleth\sqrt{\frac{a}{q}}, M = \frac{\sigma{\beta_o}^2}{a\rho}, \mathrm{Cr} = \hat{\mathrm{C}}\mathrm{r}\left(\hat{\mathrm{C}} - \hat{\mathrm{C}}_\infty\right). \tag{9}$$

After simplification.

$$f''' - (f')^2 + \left(f + \hat{\mathrm{C}}g\right)f'' + \mathcal{W}ef''f''' + gf'' - \gamma f' - Mf'(\xi) = 0, \tag{10}$$

$$g''' - (g')^2 + \left(f + \hat{\mathrm{C}}g\right)g'' + \mathcal{W}eg''g''' + fg'' - \gamma g' - Mg'(\xi) = 0, \tag{11}$$

$$\frac{1}{Pr}\left(1 + \frac{4}{3}Rd\right)\theta'' + \left(f + \hat{\mathrm{C}}g\right)\theta' + N_b\phi'\theta' + N_t(\theta')^2 - \mathrm{Cr}\theta' = 0, \tag{12}$$

$$\phi(\xi) + \bar{\mathrm{L}}e\left(f + \hat{\mathrm{C}}g\right)\phi'(\xi) + \frac{N_t}{N_b}\theta''(\xi) = 0. \tag{13}$$

With boundary conditions

$$f(0) = 0, f'(0) = 1, g'(0) = c, g'(0) = 0, f'(\infty) = 0, g'(\infty) = 0, \theta'(0) = -Bi_1\left(1 - \theta(0)\right), \phi'(0) = -Bi_2\left(1 - \phi'(0)\right), \theta(\infty) = \phi(\infty) = 0. \tag{14}$$

In the above equalities, $\mathcal{W}e = \mathrm{r}x\sqrt{2\,{a^3}/{v}}$ signifies Williamson factor, $\gamma = \frac{\nu^*}{ak^*}$ specifies the permeability constraint, $Pr = \rho v\hat{\mathrm{C}}_p/k$ shows the Prandtl figure, $Rd = 4\sigma^*\dot{\mathrm{T}}_\infty^3/kk^*$ represents the heat rays parameter$N_t = \tau_1 D_{\dot{\mathrm{T}}}(\dot{\mathrm{T}}_f - \dot{\mathrm{T}}_\infty)/q\dot{\mathrm{T}}_\infty$, $N_b = \tau_1 D_{\dot{\mathrm{T}}}(\hat{\mathrm{C}}_f - \hat{\mathrm{C}}_\infty)/q$ represent The Brownian principle plus chemical reactions motion parameters. $Bi_1 = {\hbar_f}/{k}\Big/\sqrt{{q}/{a}}$, $Bi_2 =$

$\frac{h_s}{D_B}/\sqrt{q/a}$, where Bi_1 and Bi_2 the Biot numbers. Local Nusselt number and Sherwood number, which are dimensional form, are well-defined as

$$\frac{1}{\sqrt{2}}C_f\sqrt{Re_x} = \left(f''(0) + \mathcal{W}e(f'')^2(0)\right), \tag{15}$$

$$\frac{1}{\sqrt{2}}C_f\sqrt{Re_x} = \left(g''(0) + \mathcal{W}e(g'')^2(0)\right), \tag{16}$$

$$\mathcal{P} = -\left(1 + \frac{4}{3}Rd\right)\theta'(0), Sh = -\phi'(0). \tag{17}$$

3. Solution by Homotopy Analysis Method

To explain obtained equations for the typical (10)–(17) with modelled limit Circumstances (20) we have employed stands for Homotopy Analysis Method [20-24]. The initial assumptions remain selected in the following way:

$$f_0(\xi) = 1 - e^{-\xi}, g_0(\xi) = c\left(1 - e^{-\xi}\right), \theta_0(\xi) = \left(\frac{Bi_1}{1 - Bi_1}\right)e^{-\xi}, \phi_0(\xi) = \left(\frac{Bi_2}{1 - Bi_2}\right)e^{-\xi}. \tag{18}$$

The $\mathcal{L}_f, \mathcal{L}_g, \mathcal{L}_\theta$ and $\mathcal{L}_\phi$ are linear algorithms that are obtained

$$\mathcal{L}_f(f) = f''' - f', \mathcal{L}_g(g) = g''' - g', \mathcal{L}_\theta(\theta) = \theta'' - \theta, \mathcal{L}_\phi(\phi) = \phi'' - \phi, \tag{19}$$

which have the succeeding properties:

$$\mathcal{L}_f\left(\Psi_1 + \Psi_2 e^{-\xi} + \Psi_3 e^{\xi}\right) = 0, \mathcal{L}_g\left(\Psi_4 + \Psi_5 e^{-\xi} + \Psi_6 e^{\xi}\right) = 0, \mathcal{L}_\theta\left(\Psi_7 e^{-\xi} + \Psi_8 e^{\xi}\right) = 0, \mathcal{L}_\phi\left(\Psi_9 e^{-\xi} + \Psi_{10} e^{\xi}\right) = 0. \tag{20}$$

Where $\Psi_1, \Psi_2, \Psi_3, \Psi_4, \Psi_5, \Psi_6, \Psi_7, \Psi_8, \Psi_9, \Psi_{10}$ are fixed numbers.

4. Discussion

This portion has given the influences of emerging parameters. The parameters that emerge basic parameters for bending (c), Williamson factor $(\mathcal{W}e)$, Porosity factor (γ), Heat rays factor (Rd), Prandtl number (Pr), thermophoresis factor N_t Brownian motion factor N_b and Biot numbers (Bi_1, Bi_2) on velocities profiles $(f_0(\xi), g_0(\xi))$ length, temperature profile $\theta(\xi)$ and concentration patterns $\phi(\xi)$. $\boldsymbol{Figs.\,2}$, $\mathbf{3}$. Indicates the effect of $(\mathcal{W}e)$ on $f_0(\xi), g_0(\xi)$ in the $x-$ and $y-$ direction correspondingly. The relaxing interval divided by the retardation interval is this parameter. The further the Williamson factor is increased the greater is the relaxation interval. Due to this, the fluid viscosity heightens, which consequently the rate of fluid components decreases. $\boldsymbol{Figs.\,4, 5}$. Shows the falling velocity profile with increase in magnetic restriction upsurge. The liquid and tiny fluid particles that move in the carrier are both slowed by

the magnetic field. The magnetic parameter is a pure number that is utilized in momentum equations attributed to the Lorentz force concept. It is found that the Lorentz force is negative. It is this adverse effect that pushes the reduction of velocity curves. The magnetic field is believed to be physically in anti-flow direction. The rate of the fluid elements thus reduces. The negative Lorentz force, therefore, decreases the flow of fluid particles. Velocity curves drop as a result of a electromagnetic field. A electromagnetic field attracts the charged particles of a fluid to a fluid resulting in the Lorentz force pulling the fluid. The stronger electromagnetic pitch squeezer-compresses the fluid reducing its velocity and cross-sectional area. $\boldsymbol{Figs.6,7}$ Demonstrations the sway of (γ) on $f_0(\xi), g_0(\xi)$. The permeable moderate has effects on the boundary layer that causes acceleration to the fluid. Because of this circumstance, the rate shape decreases by the increase of the absorbency factor. $\boldsymbol{Fig.8}$ demonstrates the influence the Brownian diffusion that is practically linked to the expected motion of nanomaterial and runs. $\boldsymbol{Fig.9}$ indicates that an increase in the factor N_b of Brownian indication enhances the random motion of the fluid particles, increases heat generation and reduces the fluid concentration. The higher the thermophoresis parameter, the more concentrated profile. As seen in $\boldsymbol{Fig.10}$, The thermophoresis process increased parameters increase the temperature profile. The parameters of the thermophoresis enhance the viscosity of the thermal barrier layer that elevates the temperature of the nanoparticles. $\boldsymbol{Fig.11}$ shows the concentration boundary layer gets thicker as the thermophoresis value gets bigger. A first-rate chemical reaction leads to the decrease in the level pattern. A weaker focus of the reactive substances close to the surface to the fluid is exposed. K determines the concentration of the fluid, $\boldsymbol{Fig.12}$ shows that the temperature profile is strongly affected by a comparative study of proposed nanoparticles and that the behavior is decreasing with Pr. In fluid dynamics and heat transfer, the Prandtl number is the ratio of diffusivity of heat to diffusion of momentum. It is dimensionless. The following are possible outcomes. Prandtl tends to grow in association with a drop in convective heat transfer. The bulk movement of the fluid is utilized in convective heat transmission to transfer heat. Prandtl amount is a proportion of the significance of diffusion of heat to fluid momentum diffusion as it increases. The efficiency of convective heat transport decreases, which makes the profile of temperature decreasing. The temperature profile in $\boldsymbol{Fig.13}$ is a very strong and increasing upward tendency induced by Thermal radiation. It has been proved that thermal radiations drive argumentation of the heat energy. The thermo radiations produce the greatest heat energy to the fluid particles. The higher the radiation the thinner are the thermal layers. As well, the

temperature side view rises when there is an effect of thermal radiation factors. Reduction in the thermal radiation parameter provides radiative heat transmission with priority over other heat transfer mechanisms. Electromagnetic radiations are generated when the mechanism temperature is increased. To ensure radiative heat transfer, the parameter of thermal radiation must be enhanced. The engineering should streamline heat conductivity in porous media, i.e. thermal insulation or energy system, by considering change in radiation and Darcy-Forchheimer factors. They have applications in the biomedical fields to construct a scaffold in tissue engineering and to improve the delivery system of drugs through the regulation of fluid flow and heat distribution in porous biological tissues. ***Fig*. 14** shows the chemical reaction reducing the profile of concentration is first-rate. A decreasing concentration of reactive substances near the surface with less intensity is exposed to the fluid. Cr is known to affect the amount of fluid, as the values of Cr get larger, the diffusion of mass becomes slow and the flow field boundary concentration becomes thinner. The concentration of the fluid thus falls with the growth in Cr. As seen in ***Fig*. 15**, the motile microbe profile declines as the bioconvection Lewis number $\bar{L}e$ value soars. Physically, bioconvection causes fluid to be drawn towards the surface pushing the mobile microorganisms of the border layer.

The effects of $\mathcal{W}e$, M and γ on skin friction are shown in **Table. 1** Skin friction increases by the increase of $\mathcal{W}e$, M and γ. The mathematical values of $-g''(0)$ and for common standards of $\mathcal{W}e$, M and γ are displayed in **Table. 2** Skin friction increases with increasing $\mathcal{W}e$ and γ and decreases with increasing M. **Table. 3** shows the Mathematical values of $-\theta'(0)$ for frequent standards of N_b, Pr, N_t and Rd. By increasing N_b, N_t and Rd the nusselt number decreases and by the increase of Pr the nusselt number increases. **Table. 4** decipts the influence of N_t, N_b, Le and Cr on reduced Sherwood number. This shows that as N_b, Le and Cr increases the reduced Sherwood number decreases but opposite behavior occurred, as there is an increase in N_t the Sherwood number increases.

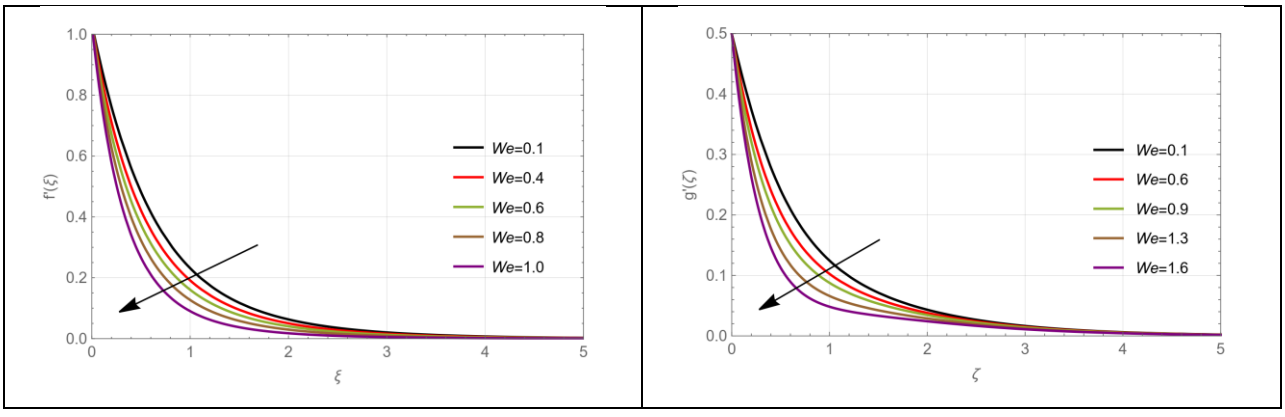

Fig. 2. The impact of Williamson parameter on patterns of velocity $\mathcal{W}e$ on $g'(\xi)$,when $M = 0.1, \gamma = 0.7$

Fig. 3. The impact of Williamson parameter on velocity patterns $\mathcal{W}e$ on $g'(\xi)$,when $M = 0.1, \gamma = 0.7$

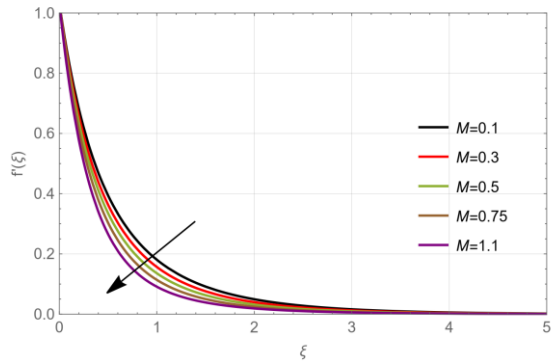

Fig. 4. The impact of Williamson parameter on velocity patterns M on $f'(\xi)$,when $\mathcal{W}e = 0.1, \gamma = 0.7$

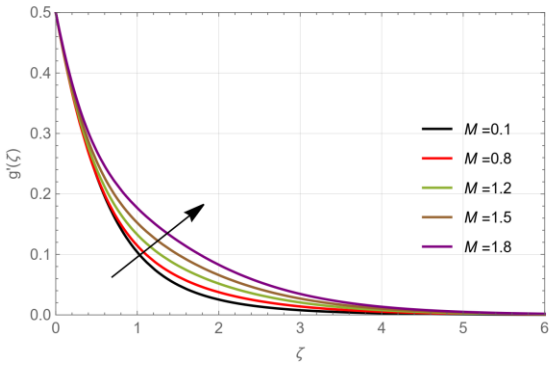

Fig. 5. The impact of Williamson parameter on velocity patterns M on $g'(\xi)$,when $\mathcal{W}e = 0.1, \gamma = 0.7$

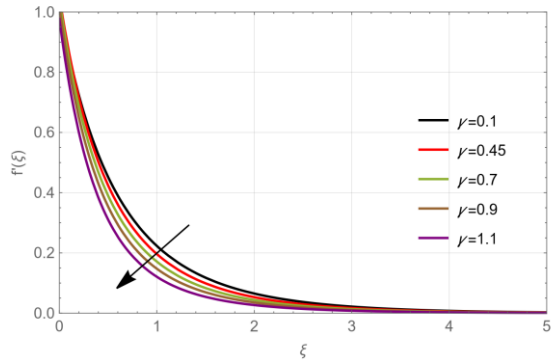

Fig. 6. Influence of (γ) on $f'(\xi)$, when $M = 0.1, \mathcal{W}e = 0.7$

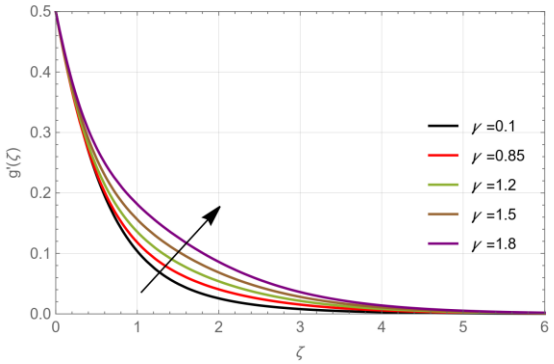

Fig. 7. Influence of (γ) on $g'(\xi)$, when $M = 0.1, \mathcal{W}e = 0.7$

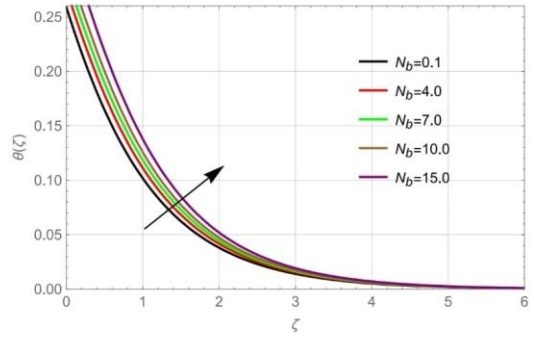

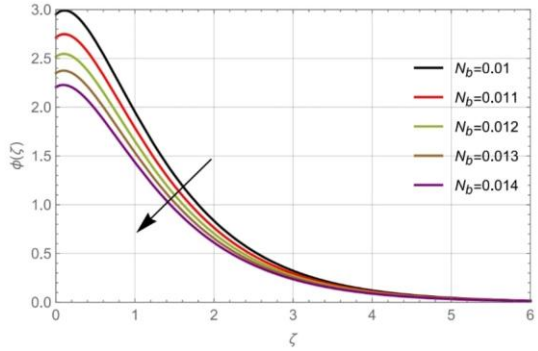

Fig. 9. Influence of the Brownian motion

Fig. 8. Influence of the Brownian motion The temperature patterns variable of N_b on $\theta(\xi)$, when $N_t = 0.1\,, Pr = 0.10\,, Rd = 0.10,$

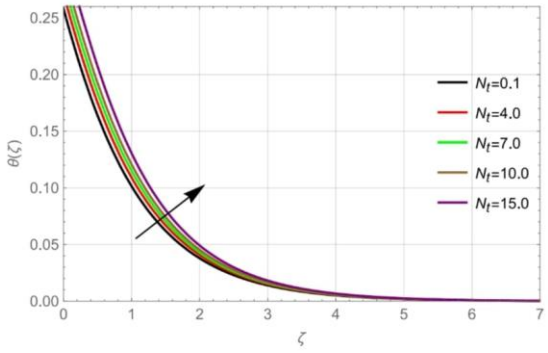

Fig. 10. Influence of the thermophoresis variables on temperature patterns of N_t on $\theta(\xi)$, when $N_b = 0.1\,, Pr = 0.10\,, Rd = 0.10,$

factor on concentration profiles of N_b scheduled $\phi(\xi)$, given $N_t = 0.35\,, \mathrm{Cr} = 0.3\,, \bar{L}e = 0.1,$

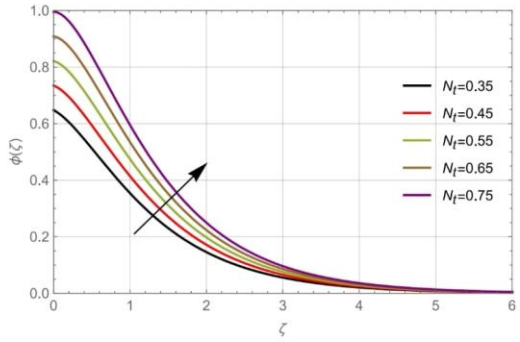

Fig. 11. Conclusion of the thermophoresis parameter scheduled concentration patterns of N_t on $\phi(\xi)$, given $N_b = 0.01\,, \mathrm{Cr} = 0.3\,, \bar{L}e = 0.1$

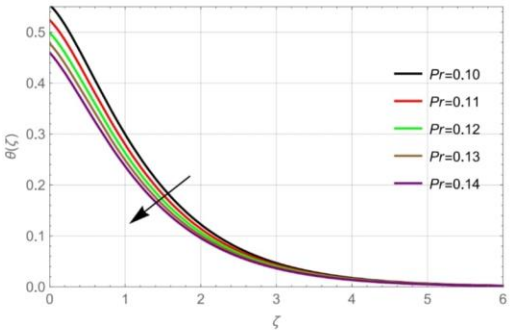

Fig. 12. Impact of the Prandtl number (Pr),on temperature profiles on $\theta(\xi)$, when $N_t = 0.1\,,$ $N_b = 0.1\,, Rd = 0.10,$

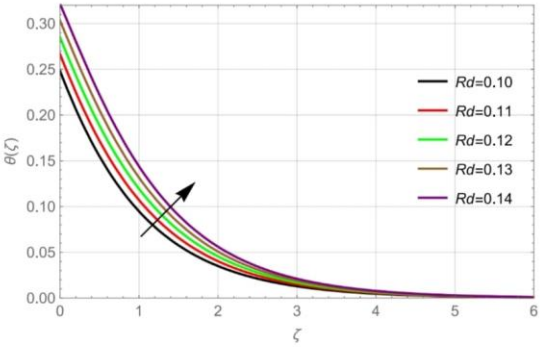

Fig. 13. Impact of the thermal radiation parameter Rd scheduled $\theta(\xi)$, when $N_t = 0.1\,, Pr = 0.10\,, N_b = 0.10,$

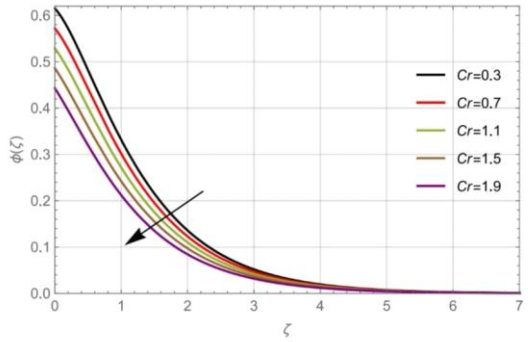

Fig. 14. Impact of the chemical response factor scheduled concentration profiles of Cr on $\phi(\xi)$, when $N_b = 0.01$, $N_t = 0.35$, $\bar{\text{L}}e = 0.1$

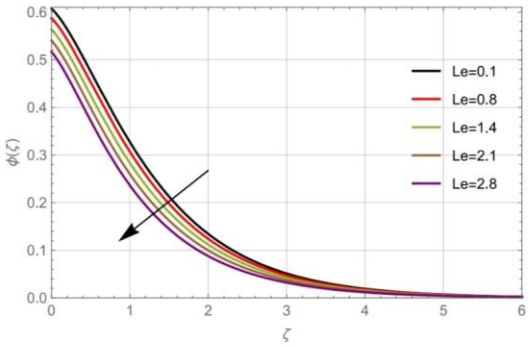

Fig. 15. Impact of the Lewis number parameter on concentration patterns of $\bar{\text{L}}e$ on $\phi(\xi)$, when $N_b = 0.01$, $N_t = 0.35$, $\text{Cr} = 0.3$

Table 1. Mathematical values of $-f''(0)$ and for frequent standards of $\mathcal{W}e, \gamma, M$.

$\mathcal{W}e$	γ	M	$\hat{\text{C}}_{fx}$ for $f''(0)$
0.1			−1.50996
0.2			−1.37702
0.3			−1.15176
0.4			−0.80738
	0.1		0.02757
	0.2		0.10178
	0.3		0.17404
	0.4		0.24322
		0.1	0.30068
		0.2	0.35553
		0.3	0.40992
		0.4	0.46366

Table 2. Mathematical values of $-g''(0)$ and for frequent standards of $\mathcal{W}e, \gamma, M$.

We	γ	M	$\hat{C}_{fy}$ for $g''(0)$
0.1			-0.66637
0.2			-0.65376
0.3			-0.63196
0.4			-0.59910
	0.1		-0.59553
	0.2		-0.60619
	0.3		-0.61575
	0.4		-0.62423
		0.1	-0.63163
		0.2	-0.63797
		0.3	-0.64324
		0.4	-0.64745

Table 3. Mathematical values of heat allocation rate for different inserted strictures $N_b, N_t, Pr, Rd.$

N_b	N_t	Pr	Rd	$-\theta'(0)$
0.1				0.25215
0.2				0.25186
0.3				0.25157
0.4				0.25129
	0.1			0.51931
	0.2			0.51907
	0.3			0.51883
	0.4			0.51859
		0.1		0.31263
		0.2		0.46537
		0.3		0.49592
		0.4		0.51629
			0.1	1.53658
			0.2	1.38336

			0.3	1.26430
			0.4	1.16823

Table 4. Mathematical values of mass allocation rate for altered various factors $N_b, N_t, \bar{L}e, \mathrm{Cr}$.

N_b	N_t	$\bar{L}e$	Cr	$-\phi'(0)$
0.1				0.36932
0.3				0.53156
0.5				0.56401
0.7				0.57791
	0.1			0.61024
	0.3			0.60538
	0.5			0.60051
	0.7			0.59564
		0.1		0.36618
		0.3		0.37246
		0.5		0.37874
		0.7		0.38501
			0.1	0.39945
			0.2	0.40949
			0.3	0.41954
			0.4	0.42958

5. Conclusions

This paper examined the $3-$ dimensional Maxwell/Williamson nanofluid movement over porous stretching surface when they are acted by combined forces of magnetohydrodynamic (MHD) forces, thermal radiation, Darcy-Forchheimer resistance, and chemical reaction. A convergent solution of governing system was found using similarity transformations and OHAM method. The findings demonstrate that MHD effects retard fluid movement and improve the temperature field because of the Lorentz force. The thermal radiation, thermophoresis, and Brownian diffusion cause a large temperature spread whereas Prandtl number suppresses it. Nanoparticle concentration reduces with a growth in chemical reaction and Schmidt figure but with thermophoresis. The drag forces decrease in the increase in porosity and the Forchheimer

number and growth in the Williamson digit. Larger values of the Prandtl figure, radiation and chemical reaction are in favor of temperature transfer and reduce under Brownian diffusion and thermophoresis. All in all, the results demonstrate the importance of MHD forces on the control of heat and momentum transfer, whereas the aspect of mass transfer in nanofluid systems falls upon the chemical reaction parameter.

- A factor that was interesting in the increase was the porosity in drag force and fall in flowing fluids in a horizontal direction;
- thermal radiation considerably affected the temperature profile, yet the other two profiles were also affected;
- The period spent relaxing of the Maxwell's design was called the Deborah number, and was found to sluggish the fluid and improved temperature and concentration profiles;
- The concentration was improved and temperature profile was reduced by Brownian diffusion;
- It appeared to be the case that the chemical reaction was a lowering factor to the nanoparticle concentration of the base fluid;
- The higher the Schmidt parameter value, the lower the concentration profile.

The strength of this study lies in its comprehensive analysis of the three-dimensional convection flow of nanofluid over a stretching sheet, considering influential factors such as MHD and chemical reaction. The practical relevance to Darcy Forchheimer adds significance to the findings. However, limitations include potential simplifications in assumptions, applicability restricted to similar geometries, assumptions about material properties, and the influence of numerical solution techniques, emphasizing the need for careful interpretation of results in specific contexts.

Acknowledgment:

We also extend our appreciation to the anonymous reviewers for their constructive feedback, which has greatly improved the quality of this paper.

Author's Declaration:

The authors declare that there is no conflict of interest regarding the publication of this paper.

Data Availablity: All data available in manuscript.

Conflicts of Intrest: On behalf of all authors, the corresponding author states that there is no conflict of interest.

References:

1. Rasool, G., Shafiq, A., Alqarni, M. S., Wakif, A., Khan, I., & Bhutta, M. S. (2021). Numerical scrutinization of Darcy-Forchheimer relation in convective magnetohydrodynamic nanofluid flow bounded by nonlinear stretching surface in the perspective of heat and mass transfer. *Micromachines*, *12*(4), 374.
2. Rasool, G., Shafiq, A., Khalique, C. M., & Zhang, T. (2019). Magnetohydrodynamic Darcy–Forchheimer nanofluid flow over a nonlinear stretching sheet. *Physica Scripta*, *94*(10), 105221.
3. Anwar, S., Rasool, G., Ashraf, M., Ahmad, U., & Sun, T. (2024). Impact of viscous dissipation and ohmic heating on natural convection heat transfer in thermo-magneto generated plume. *Frontiers in Heat and Mass Transfer*, *22*(5), 1323-1341.
4. Akbar, S., & Sohail, M. (2022). Three dimensional MHD viscous flow under the influence of thermal radiation and viscous dissipation. *Int. J. Emerg. Multidiscip. Math*, *1*(3), 106-117.
5. Rasool, G., Shafiq, A., Khalique, C. M., & Zhang, T. (2019). Magnetohydrodynamic Darcy–Forchheimer nanofluid flow over a nonlinear stretching sheet. *Physica Scripta*, *94*(10), 105221.
6. Khan, M., Irfan, M., & Khan, W. A. (2019). Heat transfer enhancement for Maxwell nanofluid flow subject to convective heat transport. *Pramana*, *92*(2), 17.
7. Khan, S. U., Shehzad, S. A., & Ali, N. (2020). Bioconvection flow of magnetized Williamson nanoliquid with motile organisms and variable thermal conductivity. *Applied Nanoscience*, *10*(8), 3325-3336.
8. Saeed, A., Tassaddiq, A., Khan, A., Jawad, M., Deebani, W., Shah, Z., & Islam, S. (2020). Darcy-Forchheimer MHD hybrid nanofluid flow and heat transfer analysis over a porous stretching cylinder. *Coatings*, *10*(4), 391.
9. Ali, B., Nie, Y., Khan, S. A., Sadiq, M. T., & Tariq, M. (2019). Finite element simulation of multiple slip effects on MHD unsteady maxwell nanofluid flow over a permeable stretching sheet with radiation and thermo-diffusion in the presence of chemical reaction. *Processes*, *7*(9), 628.
10. Ali, B., Nie, Y., Hussain, S., Manan, A., & Sadiq, M. T. (2020). Unsteady magneto-hydrodynamic transport of rotating Maxwell nanofluid flow on a stretching sheet with Cattaneo–Christov double diffusion and activation energy. *Thermal Science and Engineering Progress*, *20*, 100720.
11. Ali, F., Zaib, A., Khalid, M., Padmavathi, T., & Hemalatha, B. (2023). Unsteady MHD flow of casson fluid past vertical surface using Laplace transform solution. *Journal of Computational Biophysics and Chemistry*, *22*(03), 361-370.

12. Ali, F., Zaib, A., Khalid, M., Padmavathi, T., & Hemalatha, B. (2023). Unsteady MHD flow of casson fluid past vertical surface using Laplace transform solution. *Journal of Computational Biophysics and Chemistry*, *22*(03), 361-370.

13. Wakif, A., Boulahia, Z., & Sehaqui, R. (2018). A semi-analytical analysis of electro-thermo-hydrodynamic stability in dielectric nanofluids using Buongiorno's mathematical model together with more realistic boundary conditions. *Results in Physics*, *9*, 1438-1454.

14. Abdelsalam, S. I., & Sohail, M. (2020). Numerical approach of variable thermophysical features of dissipated viscous nanofluid comprising gyrotactic micro-organisms. *Pramana*, *94*(1), 67.

15. Uddin, I., Akhtar, R., Khan, M. A. R., Zhiyu, Z., Islam, S., Shoaib, M., & Raja, M. A. Z. (2019). Numerical treatment for fluidic system of activation energy with non-linear mixed convective and radiative flow of magneto nanomaterials with Navier's velocity slip. *AIP Advances*, *9*(5).

16. Hayat, T., Imtiaz, M., & Alsaedi, A. (2015). Effects of homogeneous-heterogeneous reactions in flow of Powell-Eyring fluid. *Journal of Central South University*, *22*(8), 3211-3216.

17. Shah, Z., Islam, S., Ayaz, H., & Khan, S. (2019). Radiative heat and mass transfer analysis of micropolar nanofluid flow of Casson fluid between two rotating parallel plates with effects of Hall current. *Journal of Heat Transfer*, *141*(2), 022401.

18. Wakif, A., Animasaun, I. L., Khan, U., Shah, N. A., & Thumma, T. (2021). Dynamics of radiative-reactive Walters-b fluid due to mixed convection conveying gyrotactic microorganisms, tiny particles experience haphazard motion, thermo-migration, and Lorentz force. *Physica Scripta*, *96*(12), 125239.

19. Jagadeesh, S., Chenna Krishna Reddy, M., Tarakaramu, N., Ahmad, H., Askar, S., & Shukhratovich Abdullaev, S. (2023). Convective heat and mass transfer rate on 3D Williamson nanofluid flow via linear stretching sheet with thermal radiation and heat absorption. *Scientific Reports*, *13*(1), 9889.

20. Akbar, S., Sohail, M., Abbas, S.T., Fouly, A. and Awwad, E.M., 2025. Entropy analysis of 3D model of non-Newtonian Williamson comprising modified heat flux and Joule heating via optimal homotopic strategy. ZAMM-Journal of Applied Mathematics and Mechanics/Zeitschrift für Angewandte Mathematik und Mechanik, 105(9), p.e70232.

21. Sultan, F., Awais, M., Sohail, M. and Mahariq, I., 2025. MHD and thermal effects on three-dimensional non-Newtonian Williamson fluid flow over a stretching sheet via numerical scheme. ZAMM-Journal of Applied Mathematics and Mechanics/Zeitschrift für Angewandte Mathematik und Mechanik, 105(8), p.e70174.

22. Sohail, M., Rafique, E., Mahariq, I. and Qureshi, I.H., 2024. Analytical investigation via OHAM on thermally magnetized non-Newtonian Williamson fluid with heat generation

and thermal radiation effects. Proceedings of the Institution of Mechanical Engineers, Part N: Journal of Nanomaterials, Nanoengineering and Nanosystems, p.23977914251338150.

23. Riaz, N., Sohail, M., Rani, A. and Mahariq, I., 2025. Engagement of OHAM to Investigate Heat and Mass Transfer in Williamson Fluid via Generalized Fluxes with Convective Boundary Conditions. Thermal Advances, p.100061.

24. Sohail, M., Waseem, F., Abodayeh, K., & Rafique, E. (2025). Analysis of entropy generation on Darcy-Forchheimer squeezed hybrid nanofluid flow between two parallel rotating disks by considering thermal radiation and viscous dissipation. Numerical Heat Transfer, Part B: Fundamentals, 1–23.